

Establishing the Catalytic Mechanism of Human Pancreatic α -Amylase with QM/MM Methods

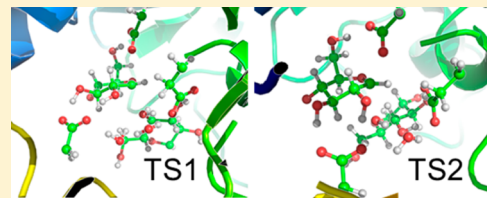
Gaspar P. Pinto,^{†,‡} Natércia F. Brás,[‡] Marta A.S. Perez,[‡] Pedro A. Fernandes,[‡] Nino Russo,[†] Maria J. Ramos,[‡] and Marirosa Toscano*,[†]

[†]Università della Calabria, Via Pietro Bucci, Arcavacata, Italia

[‡]UCIBIO, REQUIMTE, Departamento de Química e Bioquímica, Faculdade de Ciências, Universidade do Porto, Rua do Campo Alegre, s/n, 4169-007 Porto, Portugal

Supporting Information

ABSTRACT: In this work, we studied the catalytic mechanism of human pancreatic α -amylase (HPA). Our goal was to determine the catalytic mechanism of HPA with atomic detail using computational methods. We demonstrated that the HPA catalytic mechanism consists of two steps, the first of which (glycosylation step) involves breaking the glycosidic bond to culminate in the formation of a covalent intermediate. The second (deglycosylation step) consists of the addition of a water molecule to release the enzyme/substrate covalent intermediate, completing the hydrolysis of the sugar. The active site was very open to the solvent. Our mechanism basically differs from the previously proposed mechanism by having two water molecules instead of only one near the active site that participate in the mechanism. We also demonstrate the relevant role of the three catalytic amino acids, two aspartate residues and a glutamate (D197, E233, and D300), during catalysis. It was also shown that the rate limiting step was glycosylation, and its activation energy was in agreement with experimental values obtained for HPA. The experimental activation energy was 14.4 kcal mol⁻¹, and the activation energy obtained computationally was 15.1 kcal mol⁻¹.



INTRODUCTION

Human pancreatic α -amylase (HPA), an enzyme that belongs to the family of α -amylases [$\alpha(1\rightarrow 4)$ glucan-4-glucanohydrolase, EC3.2.1.1], promotes the hydrolysis of starch on $\alpha(1\rightarrow 4)$ glycosidic bonds. HPA belongs to the glycoside hydrolase (GH) family of enzymes, which catalyze the cleavage of

glycosidic bonds. This reaction, without the help of GH, would have a half-life of 5 million years. α -Amylases can be found in a large range of organisms. In humans, there are two types of α -amylase enzymes: one in the pancreas and the other in saliva. These two types differ in only 15 out of 496 amino acid residues, though some are in the active center.

The website <http://www.cazy.org>, which groups enzymes into families according to their sequence, has classified this α -amylase in the GH family number 13 within more than 100 families of enzymes described.

The α -amylases perform a wide variety of reactions involving glycosidic bonds from gly- and deglycosylation to hydrolysis and cyclization. Hyperactivity of HPA is connected to type II diabetes,^{1–3} and controlling the enzyme is of paramount importance. Hence, knowing how the enzyme works is important for designing new inhibitors that are specific to HPA.

In GH enzymes, the mechanism is said to be either retaining or inverting, and the anomeric carbon (C_1) where the reaction takes place has two possible conformations, α and β . If the initial configuration is changed after glycosidic bond breakage, the mechanism is considered to be inverting; conversely, a retaining mechanism is that in which the anomeric carbon does not change its initial stereochemistry after hydrolysis is complete.

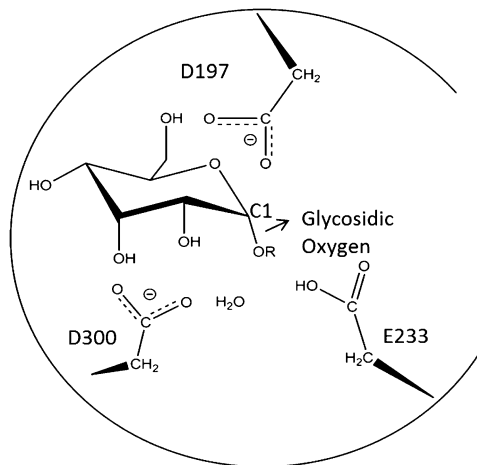


Figure 1. Quantum mechanics (QM) layer used in the enzyme/substrate conformation labeled for reference. Top to bottom: aspartate 197, anomeric carbon (C_1), glycosidic oxygen, aspartate 300, and glutamate 233. R = glucose ring.

Received: November 28, 2014

Published: May 13, 2015

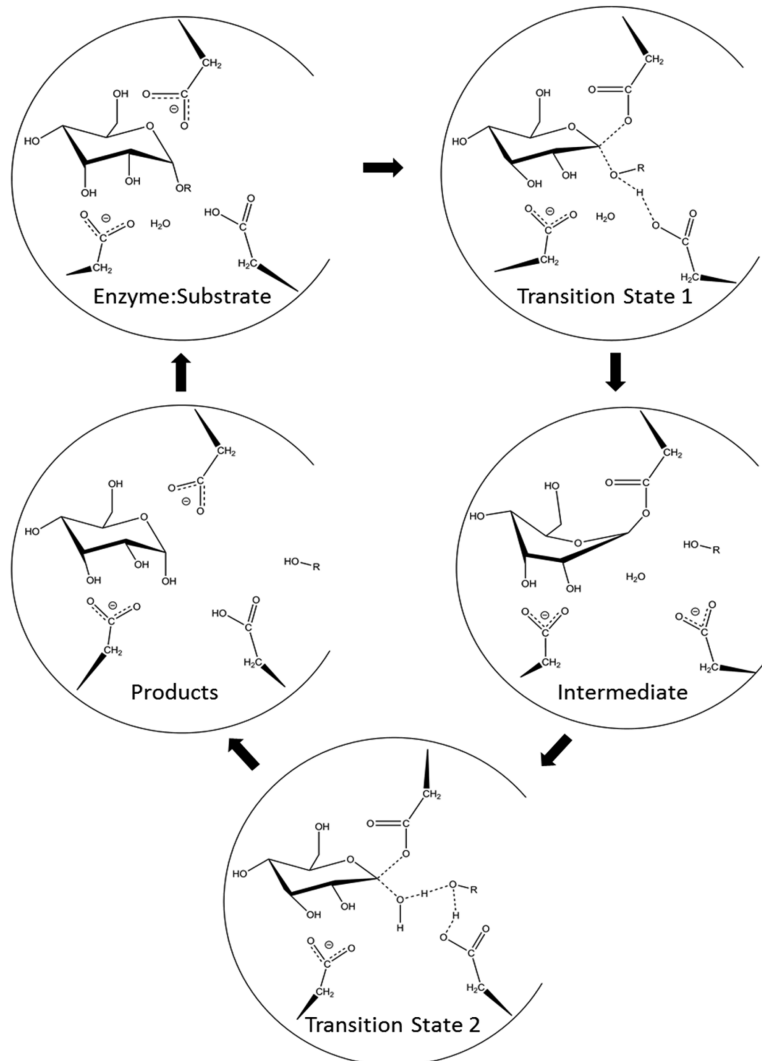


Figure 2. Proposed reaction mechanism for HPA. Residues and the substrate are in the same disposition as in Figure 1.

The general mechanism proposed for GH enzymes involves a couple of carboxylic acids (Asp and Glu residues). They catalyze the glycosylation step, thus yielding a covalent intermediate. This is followed by a nucleophilic attack from a water molecule on the anomeric carbon, forcing the covalent bond to break thus generating the deglycosylation step. Despite all of the mechanistic details already known from previous studies of other glycoside hydrolase enzymes,^{4–6} some points specific to the HPA mechanism have not yet been answered.

At the time we began our study, no structures of HPA with the natural substrate bound existed, so we determined an X-ray structure of human pancreatic amylase, the active site of which contained a docked inhibitor, which was a modified version of the commercial inhibitor Acarbose.

The amino acids that participate directly in the reaction mechanism were identified in the literature.⁴ Nevertheless, after further analysis of the active site and the interactions made by the protein with the modeled substrate, we identified one other aspartate that we found to be important in maintaining the substrate in the proper conformation for the mechanism to occur. In Figure 1, we present the active site and identify the most important amino acids.

Analyzing the tertiary structure of the enzyme, we found that the active site has a shallow pocket and that the solvent

availability was very high; thus, it was apparent that the number of water molecules that would participate in the reaction mechanism could be more than one to facilitate the second step.

The literature also tells us that one of the residues that participates actively in the mechanism should be protonated and that the other should be deprotonated, as shown in studies similar to our own, and in other mechanisms, such as those involving HIV-protease, where two amino acids in the same environment need different protonation states to initiate the mechanism.^{6–8}

Nevertheless, we decided to run a molecular dynamics (MD) simulation with both residues deprotonated. Because the active site is shallow, and with the solvent always near the substrate, it is possible that the mechanism could be initiated by a water molecule. We did not pursue this model any further with both residues deprotonated because residue E233 occupied the space near the glycosidic oxygen, blocking any water molecule that might enter the pocket deep enough to function as the proton donor (Figure 1).

Glycosidic linkages are enzymatically hydrolyzed by one of the two major groups of glycosidases: retaining and inverting.⁸ The retaining mechanism has been proposed for α -amylase,⁹ maintaining the initial conformation on the anomeric carbon.

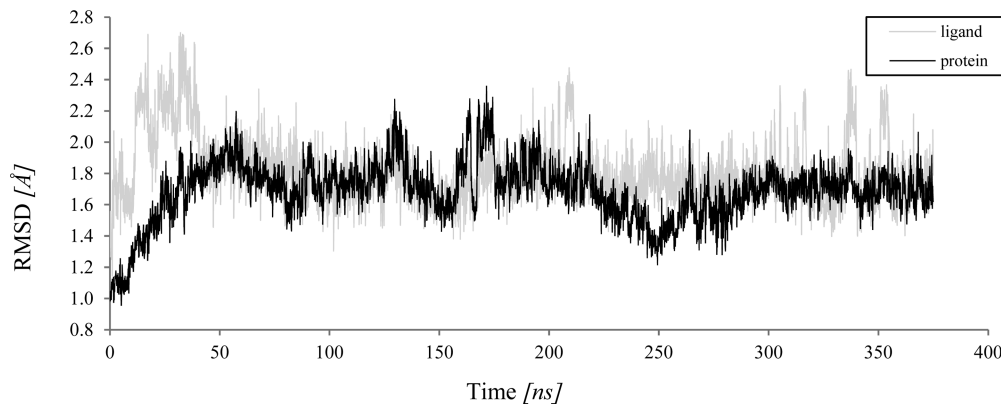


Figure 3. RMSD's of the enzyme/substrate complex, the substrate by itself, and the catalytic residues. Gray line = enzyme/substrate α carbons; black line = substrate.

In our case, however, instead of a sole pair of carboxylic acids around the anomeric carbon, there is also a third (another Asp) that stabilizes two water molecules present in the vicinity of the anomeric carbon (C_1). We have found that the presence of this second aspartate is very important; otherwise, the water molecule would be too far away to act as a nucleophile for the second mechanistic step. When starch interacts with HPA, a hydrogen bond is formed between Asp197 (nucleophilic residue) and the substrate, and the same happens with Glu233 (the proton donor group). For the transition state of the first step (TS1), it is believed that three events happen sequentially: the glycosidic bond breaks, the proton from Glu233 is transferred to the glycosidic oxygen, and anomeric carbon atom C_1 binds to nucleophile Asp197. In the end, at the intermediate geometry, there is a covalent interaction between an oxygen atom of Asp197 and the anomeric carbon. After the first mechanistic step, the water in the active site positions itself closer to C_1 , occupying the space that was previously occupied by the glycosidic oxygen. In the second mechanistic step, the water molecule promotes deglycosylation and simultaneously loses a proton that, through the glycosidic oxygen, reprotonates Glu233, as it had at the beginning of the mechanism (Figure 2).

METHODS

Models. The complex HPA/substrate was modeled from an HPA/acarbose X-ray crystallographic structure that was obtained from the PDB databank¹⁰ (ID: 1CPU⁵) with a resolution of 2.00 Å. The resulting model was used as a starting point for the computational studies. Molecular dynamics (MD) simulations were performed to evaluate the presence of water molecules near the active center and to obtain confirmation of the protonation state of the catalytic residues Asp197 and Glu233. Knowing that Asp197 was the nucleophile thus being deprotonated, two models were built with a protonated and deprotonated Glu233.

For these MD simulations, we used the amber force field (ff99sb)¹¹ and GLYCAM06¹² force field parameters for the proteins and the starch (substrate with 5 sugar rings bonded with 1–4 linkages), respectively. Explicit solvent TIP3P water in a cubic box with a minimum of 12 Å around the protein was used, and a sodium (Na^+) ion was added to neutralize the charge of the system. The resulting models consisted of 67932 and 67933 atoms for the protonated and deprotonated Glu233 systems, respectively.

Molecular Dynamics Simulations. Protonated and Deprotonated Models. For each model, we ran two

minimization steps: the first with the protein fixed and the water molecules free to move, and the second in which the whole system had no constraints. The minimized structures were then submitted to a 200 ps long warm-up simulation from 0 to 300 K at a constant volume and using periodic boundary conditions. Further, 370 ns Langevin dynamics with a 2 fs integration step were carried out. Nonbonded interactions were treated with the PME algorithm, and the cutoff was set to 10 Å, and the real part was also truncated at 10 Å with a pressure of 1 atm at 310 K with the NTP ensemble. All calculations were performed using the Amber12¹³ simulations package. Bonds involving hydrogen atoms were constrained with the SHAKE algorithm.¹⁴

Because the conformations obtained from the MD simulation for the deprotonated model showed the Glu233 far from the glycosidic oxygen and with no proton to initiate the mechanism, we ran QM/MM calculations with only the protonated model after a last minimization procedure.

QM/MM Calculations. QM/MM calculations were performed to determine the potential energy surface (PES) using Gaussian 09 software.¹⁵ The model used for the calculations was taken from the last minimization. The residues farther than 15 Å from the active site were frozen, and the water molecules from the solvent were cut off, yielding a model with a total of 7780 atoms and 505 residues. We divided our system into two layers, and the ONIOM formalism¹⁶ was used to calculate the corresponding PES. In the high layer, there were 75 atoms (i.e., two glycosidic rings, two water molecules, two aspartate side chains, and a glutamate side chain (until the β carbon)). The high layer was treated with density function theory (DFT) at the B3LYP/6-31G (d) level.^{17–21} The low layer (basically the rest of the enzyme together with the solvent water molecules) was treated at the molecular mechanics level with the parameters of the amber force field package. We used electrostatic embedding to treat the coupling between both layers.

To find transition states, we used flexible scans. The scans were made along the bond between the glycosidic oxygen and the acidic proton of Glu233 (first step) and along the bond between the water oxygen and the anomeric carbon of the covalent intermediate. Every residue within 15 Å of the active site was free, and the remaining residues were frozen. After the geometries of the transition states were roughly known, optimizations were carried out for the transition states. To ensure that the minima found corresponded to the same

reaction coordinates as the transition states, intrinsic reaction coordinate (IRC) calculations were made.

The zero point energies were calculated at the same QM/MM level as the geometry optimizations within the harmonic approximation. Thermal corrections (at 310 K) and entropies were calculated within the ideal gas/rigid rotor/harmonic oscillator model.

Single point energy calculations were performed subsequently with different density functionals (BB1K, M06, and B98),^{22–26} known to perform very well for thermodynamics and kinetics, together with the larger 6-311++G(2d,2p) basis set. Further dispersion calculations were carried for the B3LYP functional and M06. Charges were calculated through NBO analysis.^{27–32} H++ software was used to calculate the energetic cost of protonating the Glu233 in a biological environment.

RESULTS AND DISCUSSION

Because the initial file obtained from the PDB was an enzyme/acarbose complex, we had to model the natural substrate for

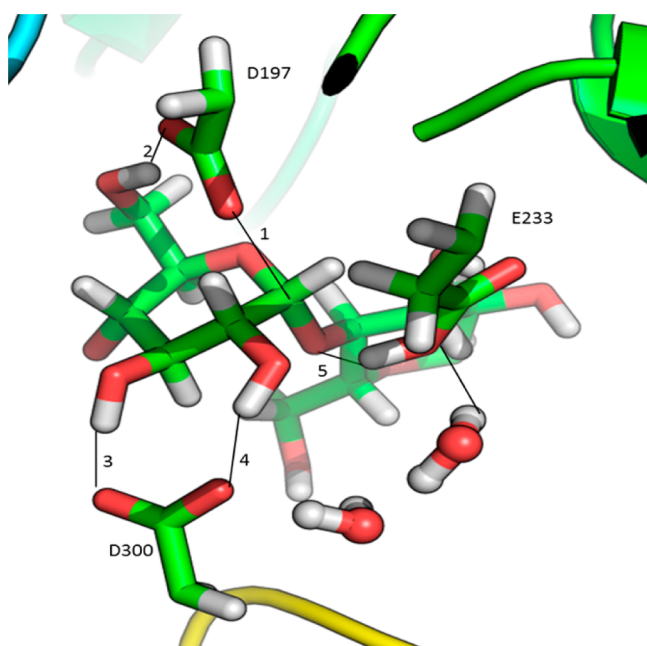


Figure 4. Reactant's three-dimensional structure of the active site with distances (Å) of the anomeric carbon to the nucleophilic residue.

HPA into the active site. As this was done manually, we performed an MD simulation to overcome any unfavorable interactions between the modeled substrate and the enzyme.

The structure of acarbose (active ingredient of some antidiabetic commercial drugs) has three glucose rings and a 4,5,6-trihydroxy-3-(hydroxymethyl) cyclohex-2-en-1-yl amine. The modified version has another glucose bonded to the cyclohexene. Being so similar to the actual substrate, the inhibitor that was already in place was logically used to model the substrate. Figure 1 shows that, even after the minimizations and molecular dynamics simulations, the modeled starch has a geometry very similar to that of the inhibitor. Certain differences are visible, as there should be because there are differences in the structures of both compounds, such as the presence of a nitrogen atom where the substrate has an oxygen atom, the absence of an oxygen atom in one cycle, and a hydroxyl group in another.

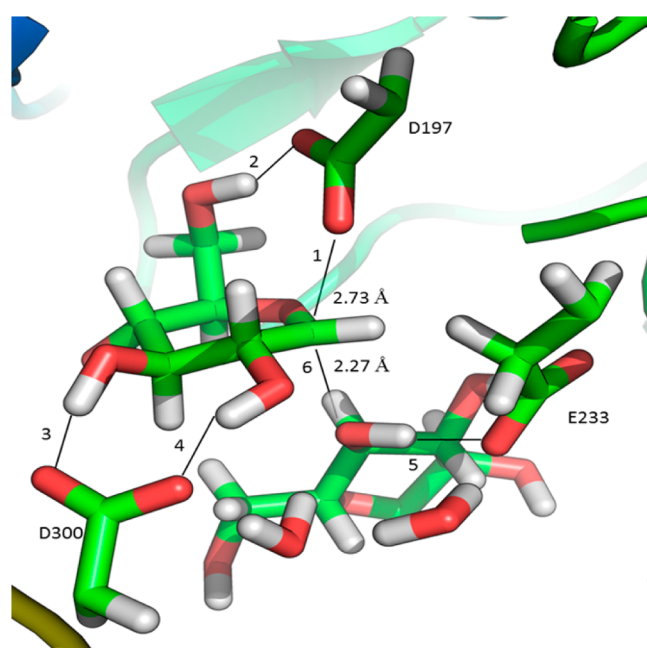


Figure 5. Transition state 1 three-dimensional structure of the active site with the distances (Å) of the anomeric carbon to the nucleophilic residue and the anomeric carbon to the glycosidic oxygen.

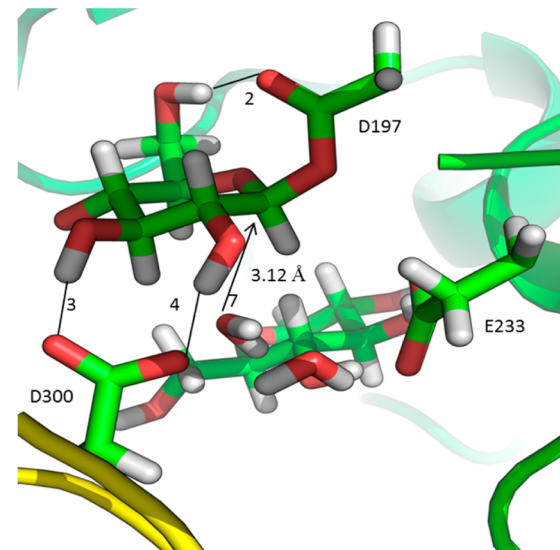


Figure 6. Intermediary with the oxygen (from water molecule)/anomeric carbon distance shown.

Obviously starch does not consist of only five glucose rings, it is a polymer that can have more than five hundred monomers (glucose rings), but it is useless to simulate such a big substrate as only two of the glucose units are involved in the catalytic mechanism, so we modeled just 5 glucose rings.

After 350 ns of the production MD simulation, when the root-mean-square deviation (RMSD) for the whole enzyme was already stabilized and not higher than 1.5 Å at its highest point, we stopped the simulation.

As can be seen in Figure 3, the enzyme/substrate dynamics trajectory has RMSD values between 1.6 and 2.0 Å over time. The substrate has a higher deviation, but we confirmed that this was due to its sugar cycles oscillating conformations and the large mobility of the oxygen in the OH groups. One ring in

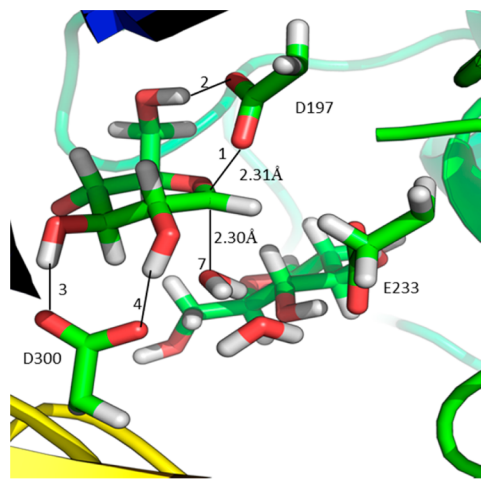


Figure 7. Second transition state with selected distances shown.

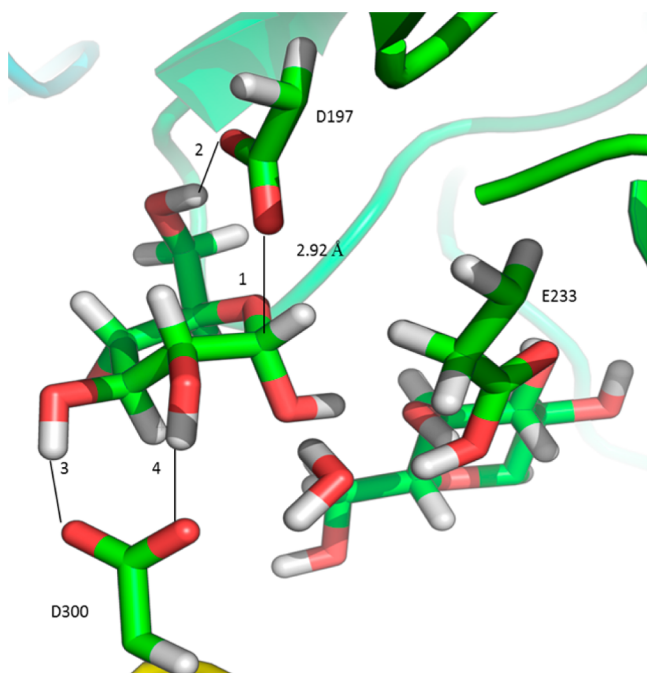


Figure 8. Products with selected distances shown.

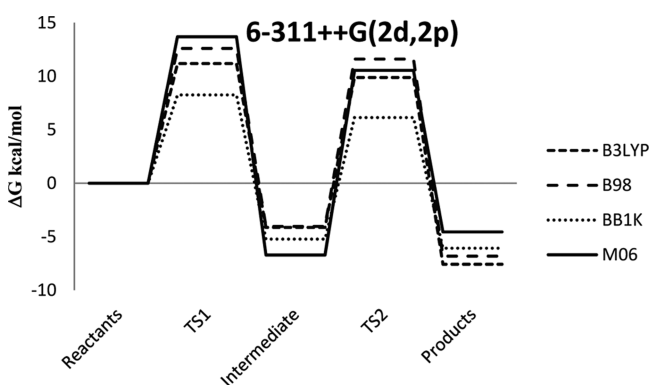


Figure 9. Potential energy surface for the HPA enzyme determined with 6-311++G(2d,2p) basis sets using four density functionals. The results were obtained from single point calculations.

particular, in position +3, has a conformational change at ~ 20 ns, but at 50 ns, it reverts back to its initial conformation. It is worth noting that this ring is in full contact with the solvent. We also noted that in the X-ray structure the temperature factors are higher in this area. The substrate interacts extensively with the side chains of amino acids in the active site, and therefore, it never leaves it during the simulation.

Analyzing the conformations obtained in the MD simulation, we saw that the substrate and its environment did not suffer big changes relatively to the initial conformation. Consequently, we proceeded to the QM/MM calculations with the conformation obtained in the last minimization procedure.

Glycosylation Step. After analyzing the reactant structure, we observed that the substrate in the active site was involved in four very strong hydrogen bonds; residue D300 established two hydrogen bonds (3 and 4 in Figure 4, represent 1.68 and 1.86 Å, respectively) with one of the sugar cycles, helping to keep it in the correct position for catalysis.

The E233 carboxylate also established two hydrogen bonds with the oxygen of the substrate, one as a donor atom (5 in Figure 4, represents 2.70 Å). The nucleophilic residue D197 looked like it was embracing the sugar ring that was going to lose the glycosidic oxygen (in Figure 4, it is making a hydrogen bond with residue E233).

One oxygen atom of D197 established a bridge with a hydroxyl group (2 in Figure 4, represents 1.81 Å), and the other oxygen atom was in a good position to attack the anomeric carbon (1 in Figure 4, represents 3.53 Å). The two water molecules that worked as a proton exchange network in the second step were positioned near the active site. Although they did not participate in the first step, they were near the active site and were stabilized between the D300 and E233 residues.

The HPA enzymatic mechanism is a retaining mechanism, meaning that the anomeric configuration of the substrate is maintained in the product. This means that the hydrolysis of the anomeric carbon should come from the alpha side of the anomeric carbon. The position of the water molecules, close to the residue Glu233, told us that those water molecules were important for the mechanism.

The proximity of the nucleophilic residue (D197) was of extreme importance for the first step to occur. It forced the anomeric carbon–glycosidic oxygen bond to break and the subsequent transfer of the proton from the E233 residue to the D197 glycosidic oxygen.

As the nucleophilic D197 residue attacked the anomeric carbon, the glycosidic bond began to extend until it reached a breaking point (6 in Figure 5) and carbon atom C1 started to bond with the aspartate (1 in Figure 5). Simultaneously, the proton bonded to the oxygen belonging to acid/base residue E233 (Figure 2) began to elongate. At this point, the anomeric carbon reached its breaking point. The proton immediately bonded to the glycosidic oxygen, as number 5 of Figure 5 shows, where the proton is already bonded to the glycosidic oxygen.

As a consequence of the D197 advance toward the anomeric carbon, the sugar ring had to adapt to the structural changes. While going from the reactant conformation to the TS1 conformation, the sugar ring changed from a stable chair conformation to a less stable half-chair conformation. Additionally, the anomeric carbon changed places until it reached a near planar angle with carbon C2 and the oxygen atom of the ring.

Table 1. Activation and Reaction Energies Obtained with Four Density Functionals and 6-311++G (2d,2p) as the Basis Set^a

6-311++G(2d,2p)	ΔG (ΔE) (kcal/mol)			
	TS1	intermediate	TS2	products
B3LYP	11.2 (14.0)	-4.1 (-3.2)	9.9 (12.1)	-7.6 (-5.9)
B98	12.6 (14.8)	-4.0 (-2.9)	11.6 (13.4)	-6.8 (-5.5)
BB1K	8.3 (9.8)	-5.2 (-4.0)	6.1 (7.4)	-6.1 (-5.3)
M06	13.7 (14.8)	-6.7 (-5.2)	10.5 (11.4)	-4.6 (-3.9)

^aThermal corrections and zero point energies were calculated for every stationary point and transition state. Electronic energies are shown in parentheses.

Table 2. Activation and Reaction Energies Obtained with Four Density Functionals and 6-31G (d) as the Basis Set^a

6-31G(d)	ΔG (kcal/mol)			
	TS1	intermediate	TS2	products
B3LYP	13.9	-8.8	8.0	-8.6
B98	15.2	-8.4	9.8	-7.9
BB1K	11.1	-8.8	4.8	-7.1
M06	17.7	-9.8	10.0	-5.1

^aThermal corrections and zero point energies were calculated for every stationary point and transition state.

NBO analysis gave us insight on point charges in every minima and transition state, thus confirming the dissociative nature of the transition state that was shown for similar enzymes in another study.⁴

The sugar ring changed back to the more stable chair conformation once the glycosylation intermediate was obtained. The anomeric carbon formed a covalent bond with the aspartate (see 1 in Figure 3 and Figure 6), yielding a very stable stationary state. The sugar ring was in its most stable conformation, the bond with D197 residue's oxygen was strong, and Figure 6 shows also the hydrogen bond established between the 6'-hydroxyl group of the sugar and one oxygen atom of the D197 residue (2 in Figure 6, represents 2.01 Å), which already existed at the beginning of the reaction. This H-bridge promoted the formation of a cycle with nine atoms with the weakest link being this hydrogen bridge between an OH group and the D197 residue.

On the alpha side of the sugar, one of the water molecules came close to where the leaving sugar was before (7 in Figure 4). This forced the leaving group to move farther away from its initial position. The second water molecule established H-bridges with residues E233 and D300.

Deglycosylation Step. In the second step of this reaction mechanism, the type of the reaction (retaining or inverting) is defined. HPA was already specifically known to be a retaining mechanism, meaning that the anomeric carbon maintains its initial isomeric configuration. This occurs when the water molecule attacks the anomeric carbon (7 in Figure 4) on the alpha side of the sugar ring.

In Figure 4, the water molecule and the D197 residue, resulting from the first mechanistic step, are on opposite sides

of the sugar ring. D197 is in a beta position, and the water molecule is in an alpha position.

These two residues, the water and the aspartate, with the anomeric carbon in the middle, form an angle of 140°. Chemically speaking, this kind of S_N2 reaction is more favorable with an angle of 180°, but in a biological medium such an angle becomes too difficult to achieve because of steric constraints around the reaction site.

Interestingly, the first mechanistic step is also an S_N2 reaction, but the angle (159°) formed by the glycosidic oxygen, the anomeric carbon, and the aspartate is closer to the ideal angle for these reactions.

From this stable stationary state, the mechanism continued with two events happening almost simultaneously: as the oxygen of the water molecule approached the anomeric carbon, both of its hydrogen–oxygen bonds extended. Concomitantly, the covalent bond between the anomeric carbon and the aspartate started to break, initiating deglycosylation. As Figure 7 shows, the transition state was reached when the anomeric carbon was halfway between the water and the aspartate. As with the first mechanistic step, the sugar ring twisted its preferred chair conformation into a half-chair. At that moment, one proton from the water molecule broke away from the oxygen atom (8 in Figure 7) and approached the second water molecule, and consequently one proton of the second water molecule moved toward the E233 residue.

After the second transition state, the sugar ring adopted a stable chair conformation with a hydroxyl group bonded to the anomeric carbon in an alpha position, thus retaining the initial conformation (Figure 8). The second water molecule reprotonates the glutamate in the active site.

Having achieved a computational mechanism similar to that proposed for HPA and similar to other glycosidase enzymes, we compared the experimental value for the energy barrier with the energy barrier obtained in this work. Previously described, the experimental activation energy of the HPA mechanism is 14.4 kcal mol⁻¹.³³

In Figure 9, we present the single point calculations with four hybrid GGA density functionals with a triple- ζ basis set with diffuse orbitals (values are shown in Table 1). Frequencies for every stationary point and transition state were computed; thus, the results presented have zero point and thermal corrections. We see in Figure 9 that the activation energies obtained for each functional are lower than the experimentally obtained

Table 3. Activation and Reaction Energies Obtained with and without the Insertion of DFT-D3 Interactions

	ΔG (kcal/mol)			
	TS1	intermediate	TS2	products
B3LYP-D3 (B3LYP)	10.0 (11.2)	-4.2 (-4.1)	8.9 (9.9)	-3.8 (-7.6)
M06D3 (M06)	13.0 (13.7)	-6.3 (-6.7)	10.6 (10.5)	-3.4 (-4.6)

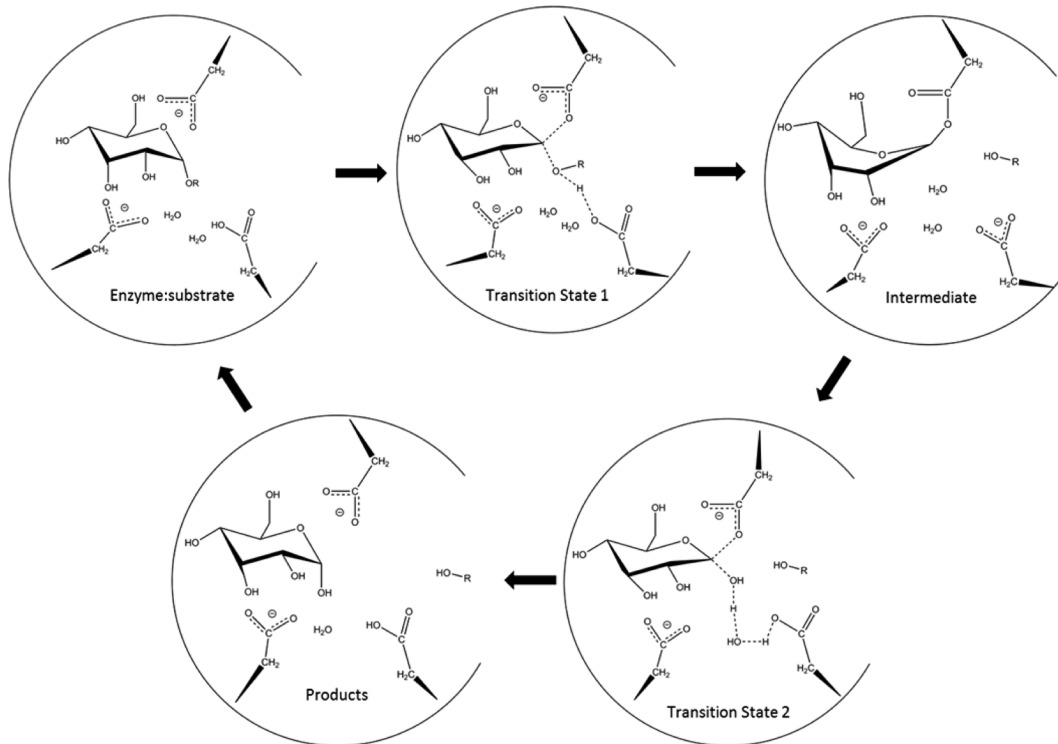


Figure 10. Mechanism obtained computationally in this work.

activation energy for this enzyme but are still within the error range given by the method. The same calculations were made with a lower level basis set as shown in Table 2. With a double- ζ basis set without diffuse orbitals, the activation energy rises for every density functional. Because the active site of our enzyme has various oxygen atoms in both carboxyl and hydroxyl groups, as well as two water molecules, a destabilization of the energy in the transition states was expected.

Analyzing the PES of both basis sets, we notice that even though TS1 has a higher ΔG , the rate limiting step is TS2 because of the intermediate stability. This is also in agreement with other glycosidase mechanisms. Both hybrid functionals yielded similar ΔG values for the activation energy with the lower basis set yielding slightly higher results.

Dispersion interactions were treated with DFT-D3 for B3LYP and M06, the results and how they compare with the results obtained without the insertion of DFT-D3 are shown in Table 3. The first transition state is stabilized, and the product energy is elevated. The intermediate has a very small elevation in the energy, and only in the second transition state is there a noticeable difference in the results obtained for both density functionals. In B3LYP, the second transition state is stabilized as it was for the first transition state; however, the second transition state ends up being slightly destabilized.

CONCLUSIONS

Despite the number of mechanistic studies performed on the glycosidase family of enzymes, a vast number of them are not understood or known in atomistic detail and require further study. In our work, we carried out a QM/MM (DFT:AMBER) study on the full enzyme to fully understand the catalytic mechanism and solvent availability near the active site. The active site has a high solvent availability, which supports our catalytic mechanism with two water molecules instead of only

one for the proposed mechanism. As is generally accepted for glycosidase enzymes, our analysis of the minima and transition states for this reaction mechanism yields a dissociative character for the transition state of the glycosylation step: the bond between the anomeric carbon and the glycosidic oxygen was at a breaking point at 2.26 Å; however, the glycosylation bond was still far (2.73 Å) from being formed.

In the second transition state, the water molecule was still not activated even though the anomeric carbon was midway between the previous glycosidic linkage and the water molecule's oxygen. Both protons had elongated bonds, but they were still both clearly bonded to the nucleophilic oxygen. In fact, only when one proton broke away was the oxygen from the former water molecule in a strong enough position to bond with the anomeric carbon, hydrolyze the sugar ring, and thus finish the second mechanistic step.

The reprotonation of the acid/base residue occurred through a water molecule. This is a change from the literature-proposed pathway for HPA (Figure 10). The activation energy is in total agreement with the experimental values in which the energy barrier is 14.4 kcal mol⁻¹.

DFT calculations yielded an activation energy of 11.2 kcal/mol. With the addition of the energetic cost of protonating Glu233, the activation energy rises to 15.1 kcal/mol, which is still in agreement with the experimental values.³³

ASSOCIATED CONTENT

S Supporting Information

Superposition of the original inhibitor with the modeled substrate, superposition of the inhibitor with the modeled substrate in the conformation that we began in this study, a table with distances obtained through IRC of the first transition state, where we see clearly that TS1 is closer to the ES geometry than the intermediate geometry. The Supporting Information is

available free of charge on the ACS Publications website at DOI: 10.1021/acs.jctc.5b00222.

AUTHOR INFORMATION

Corresponding Author

*E-mail: marirosa.toscano@unical.it.

Notes

The authors declare no competing financial interest.

ACKNOWLEDGMENTS

This work has been funded by FEDER/COMPETE and Fundação para a Ciência e a Tecnologia through Grants PEST-C/EQB/LA0006/2011 and EXCL/QEQ-COM/0394/2012. N.F.B. thankfully acknowledges her Fundação para a Ciência e Tecnologia grant (IF/01355/2014).

REFERENCES

- (1) deSales, P. M.; deSouza, P. M.; Simeoni, L. A.; Magalhaes, P. D. O.; Silveira, D. α -Amylase inhibitors: a review of raw material and isolated compounds from plant source. *J. Pharm. Pharm. Sci.* **2012**, *15*, 141–183.
- (2) Funke, I.; Melzing, M. F. Traditionally used plants in diabetes therapy – phytotherapeutics as inhibitors of α -amylase activity. *Rev. Bras. Farmacogn.* **2006**, *16*, 1–5.
- (3) Jayaraj, S.; Suresh, S.; Kadeppagari, R. K. Amylase inhibitors and their biomedical applications. *Starch/Staerke* **2013**, *65*, 535–542.
- (4) Bras, N. F.; Fernandes, P. A.; Ramos, M. J. QM/MM Studies on the α -Galactosidase Catalytic Mechanism: Hydrolysis and Trans-glycosylation Reactions. *J. Chem. Theory Comput.* **2010**, *6*, 421.
- (5) Passos, O.; Fernandes, P. A.; Ramos, M. J. QM/MM Study of the Catalytic Mechanism of GalNAc Removal from GM2 Ganglioside Catalyzed by Human β -Hexosaminidase A. *J. Phys. Chem. B* **2011**, *115*, 14751–14759.
- (6) Bras, N. F.; Ramos, M. J.; Fernandes, P. A. DFT studies on the β -glycosidase catalytic mechanism: The deglycosylation step. *J. Mol. Struct.: THEOCHEM* **2010**, *946*, 125–133.
- (7) Brik, A.; Wong, C. H. HIV-1 protease: mechanism and drug discovery. *Org. Biomol. Chem.* **2003**, *1*, 5–14.
- (8) Chiba, S. A Historical Perspective for the Catalytic Reaction Mechanism of Glycosidase; So as to Bring about Breakthrough in Confusing Situation. *Biosci. Biotechnol. Biochem.* **2012**, *76*, 215–231.
- (9) Zhang, R.; Li, C.; Williams, L. K.; Rempel, B. P.; Brayer, G. D.; Withers, S. G. Directed “in Situ” Inhibitor Elongation as a Strategy To Structurally Characterize the Covalent Glycosyl-Enzyme Intermediate of Human Pancreatic α -Amylase. *Biochemistry* **2009**, *48*, 10752–10764.
- (10) Bernstein, F. C.; Koetzle, T. F.; Williams, G. J.; Meyer, E. E., Jr.; Brice, M. D.; Rodgers, J. R.; Kennard, O.; Shimanouchi, T.; Tasumi, M. The Protein Data Bank: A Computer-based Archival File for Macromolecular Structures. *J. Mol. Biol.* **1977**, *112*, 535–542.
- (11) Brayer, G. D.; Sidhu, G.; Maurus, R.; Rydberg, E. H.; Braun, C.; Wang, Y.; Nguyen, N. H.; Overall, C. M.; Withers, S. G. Subsite Mapping of the Human Pancreatic α -Amylase Active Site through Structural, Kinetic, and Mutagenesis Techniques. *Biochemistry* **2000**, *39*, 4778–4791.
- (12) Hornak, V.; Abel, R.; Okur, A.; Strockbine, B.; Roitberg, A.; Simmerling, C. Comparison of multiple Amber force fields and development of improved protein backbone parameters. *Proteins* **2000**, *65*, 712–725.
- (13) Kirschner, K. N.; Yonge, A. B.; Tschampel, S. M.; Outeiro, J. G.; Daniels, C. R.; Foley, B. L.; Woods, R. J. GLYCAM06: A generalizable biomolecular force field. *Carbohydrates. J. Comput. Chem.* **2008**, *29*, 622–655.
- (14) Case, D. A.; Darden, T. A.; Cheatham, T. E.; Simmerling, C. L.; Wang, J.; Duke, R. E.; Luo, R.; Walker, R. C.; Zhang, W.; Merz, K. M.; Roberts, B.; Hayik, S.; Roitberg, A.; Seabra, G.; Swails, J.; Goetz, A. W.; Kolossvary, I.; Wong, K. F.; Paesani, F.; Vanicek, J.; Wolf, R. M.; Liu, J.; Wu, X.; Brozell, S. R.; Steinbrecher, T.; Gohlke, H.; Cai, Q.; Ye, X.; Wang, J.; Hsieh, M. J.; Cui, G.; Roe, D. R.; Mathews, D. H.; Seetin, M. G.; Salomon-Ferrer, R.; Sagui, C.; Babin, V.; Luchko, T.; Gusarov, S.; Kovalenko, A.; Kollman, P. A. AMBER 12; University of California: San Francisco, CA, 2012.
- (15) Hammonds, K. D.; Ryckaert, J. P. On the convergence of the SHAKE algorithm. *Comput. Phys. Commun.* **1991**, *62*, 336–351.
- (16) Frisch, M. J.; Trucks, G. W.; Schlegel, H. B.; Scuseria, G. E.; Robb, M. A.; Cheeseman, J. R.; Scalmani, G.; Barone, V.; Mennucci, B.; Petersson, G. A.; Nakatsuji, H.; Caricato, M.; Li, X.; Hratchian, H. P.; Izmaylov, A. F.; Bloino, J.; Zheng, G.; Sonnenberg, J. L.; Hada, M.; Ehara, M.; Toyota, K.; Fukuda, R.; Hasegawa, J.; Ishida, M.; Nakajima, T.; Honda, Y.; Kitao, O.; Nakai, H.; Vreven, T.; Montgomery, J. A., Jr.; Peralta, J. E.; Ogliaro, F.; Bearpark, M.; Heyd, J. J.; Brothers, E.; Kudin, K. N.; Staroverov, V. N.; Kobayashi, R.; Normand, J.; Raghavachari, K.; Rendell, A.; Burant, J. C.; Iyengar, S. S.; Tomasi, J.; Cossi, M.; Rega, N.; Millam, M. J.; Klene, M.; Knox, J. E.; Cross, J. B.; Bakken, V.; Adamo, C.; Jaramillo, J.; Gomperts, R.; Stratmann, R. E.; Yazyev, O.; Austin, A. J.; Cammi, R.; Pomelli, C.; Ochterski, J. W.; Martin, R. L.; Morokuma, K.; Zakrzewski, V. G.; Voth, G. A.; Salvador, P.; Dannenberg, J. J.; Dapprich, S.; Daniels, A. D.; Farkas, Ö.; Foresman, J. B.; Ortiz, J. V.; Ciosowski, J.; Fox, D. J., Gaussian 09, revision D.01; Gaussian Inc.: Wallingford, CT, 2009.
- (17) Dapprich, S.; Komáromi, I.; Byun, K. S.; Morokuma, K.; Frisch, M. J. A New ONIOM Implementation in Gaussian 98. Part 1. The Calculation of Energies, Gradients and Vibrational Frequencies and Electric Field Derivatives. *J. Mol. Struct.: THEOCHEM* **1999**, *462*, 1–21.
- (18) Becke, A. D. Density-functional thermochemistry. III. The role of exact exchange. *J. Chem. Phys.* **1993**, *98*, 5648–5652.
- (19) Lee, C.; Yang, W.; Parr, R. G. Development of the Colle-Salvetti correlation-energy formula into a functional of the electron density. *Phys. Rev. B* **1988**, *37*, 785–789.
- (20) Vosko, S. H.; Wilk, L.; Nusair, M. Accurate spin-dependent electron liquid correlation energies for local spin density calculations: a critical analysis. *Can. J. Phys.* **1980**, *58*, 1200–1211.
- (21) Stephens, P. J.; Devlin, F. J.; Chabalowski, C. F.; Frisch, M. J. Ab Initio Calculation of Vibrational Absorption and Circular Dichroism Spectra Using Density Functional Force Fields. *J. Phys. Chem.* **1994**, *98*, 11623–11627.
- (22) Becke, A. D. Density-functional thermochemistry. IV. A new dynamical correlation functional and implications for exact-exchange mixing. *J. Chem. Phys.* **1996**, *104*, 1040–1046.
- (23) Zhao, Y.; Truhlar, D. G. The M06 suite of density functionals for main group thermochemistry, thermochemical kinetics, non-covalent interactions, excited states, and transition elements: two new functionals and systematic testing of four M06-class functionals and 12 other functionals. *Theor. Chem. Acc.* **2008**, *120*, 215–241.
- (24) Schmid, H. L.; Becke, A. D. Optimized density functionals from the extended G2 test set. *J. Chem. Phys.* **1998**, *108*, 9624–9631.
- (25) Foster, J. P.; Weinhold, F. Natural hybrid orbitals. *J. Am. Chem. Soc.* **1980**, *102*, 7211–7218.
- (26) Zhao, Y.; Lynch, B. J.; Truhlar, D. G. Development and Assessment of a New Hybrid Density Functional Method for Thermochemical Kinetics. *J. Phys. Chem. A* **2004**, *108*, 2715–2719.
- (27) Reed, A. E.; Weinhold, F. Natural bond orbital analysis of near-Hartree–Fock water dimer. *J. Chem. Phys.* **1983**, *78*, 4066–4073.
- (28) Reed, A. E.; Weinstock, R. B.; Weinhold, F. Natural-population analysis. *J. Chem. Phys.* **1985**, *83*, 735–746.
- (29) Reed, A. E.; Weinhold, F. Natural Localized Molecular Orbitals. *J. Chem. Phys.* **1985**, *83*, 1736–1740.
- (30) Carpenter, J. E.; Weinhold, F. Analysis of the geometry of the hydroxymethyl radical by the different hybrids for different spins natural bond orbital procedure. *J. Mol. Struct.: THEOCHEM* **1988**, *46*, 41–62.
- (31) Reed, A. E.; Curtiss, L. A.; Weinhold, F. Intermolecular interactions from a natural bond orbital, donor-acceptor viewpoint. *Chem. Rev.* **1988**, *88*, 899–926.

(32) Weinhold, F.; Carpenter, J. E. *Electronic Structure-Theory. The Structure of Small Molecules and Ions*, 1st Edition; New York, NY, 1988; Vol. 1, pp 227–236.

(33) Rydberg, E. H.; Li, C.; Maurus, R.; Overall, C. M.; Brayer, G. D.; Withers, S. G. Mechanistic Analyses of Catalysis in Human Pancreatic R-Amylase: Detailed Kinetic and Structural Studies of Mutants of Three Conserved Carboxylic Acids. *Biochemistry* 2002, 41, 4492–4502.